Materials Science Forum
ISSN: 1662-9752, Vol. 885, pp 13-18
doi:10.4028/www.scientific.net/MSF.885.13

Submitted: 2016-02-02
Revised: 2016-07-14
Accepted: 2016-09-21
Online: 2017-02-10

The Influence of Plastic Deformation on Lattice Defect Structure and Mechanical Properties of 316L Austenitic Stainless Steel

Moustafa El-Tahawy[1,2,a*], Jenő Gubicza[1,b], Yi Huang[3,c], Hyelim Choi[4,d], Heeman Choe[4,e], János L. Lábár[5,f] and Terence G. Langdon[3,g]

[1] Department of Materials Physics, Eötvös Loránd University, Budapest, P.O.B. 32, H-1518, Hungary

[2] Department of Physics, Faculty of Science, Tanta University, 31527, Tanta, Egypt

[3] Materials Research Group, Faculty of Engineering and the Environment, University of Southampton, Southampton SO17 1BJ, UK

[4] School of Advanced Materials Engineering, Kookmin University, 77 Jeongneung-ro, Seongbuk-gu, Seoul 136-702, Republic of Korea

[5] Institute for Technical Physics and Materials Science, Centre for Energy Research, Hungarian Academy of Sciences, Budapest, Hungary

[a]mmt_eltahawy@yahoo.com, [b]jeno.gubicza@ttk.elte.hu, [c]Y.Huang@soton.ac.uk, [d]choihl@kookmin.ac.kr, [e]heeman@kookmin.ac.kr, [f]labar@mfa.kfki.hu, [g]langdon@usc.edu

Keywords: martensitic transformation, defect structure, steel, α'-martensite, γ-austenite.

Abstract. The effect of different plastic deformation methods on the phase composition, lattice defect structure and hardness in 316L stainless steel was studied. The initial coarse-grained γ-austenite was deformed by cold rolling (CR) or high-pressure torsion (HPT). It was found that the two methods yielded very different phase compositions and microstructures. Martensitic phase transformation was not observed during CR with a thickness reduction of 20%. In γ-austenite phase in addition to the high dislocation density (~10×10^{14} m^{-2}) a significant amount of twin-faults was detected due to the low stacking fault energy. On the other hand, γ-austenite was gradually transformed into ε and α'-martensites with transformation sequences γ→ε→α' during HPT deformation. A large dislocation density (~133×10^{14} m^{-2}) was detected in the main phase (α'-martensite) at the periphery of the disk after 10 turns of HPT. The high defect density is accompanied by a very small grain size of ~45 nm in the HPT-processed sample, resulting in an very large hardness of 6130 MPa.

Introduction

The 316L stainless steel has attracted considerable interest as it possesses high strength, good ductility, high fracture toughness, excellent corrosion and oxidation resistance, and a low neutron absorption rate [1,2]. Therefore, this material is used successfully in industrial and technological applications, including nuclear power plants and orthopaedic implants [3,4]. The strength of 316L steel can be increased with the application of plastic deformation techniques such as equal-channel angular pressing (ECAP), cold rolling (CR) or high-pressure torsion (HPT). These procedures achieve strength increments due to the production of ultrafine-grained (UFG) or nanostructured microstructures with high lattice defect densities [5,6].

It is well known that in metastable austenitic stainless steels (e.g. 316L, 301LN, 304, 304L) a martensitic transformation may occur due to plastic deformation at low temperatures [7-9]. In this phase transformation the face-centered cubic (fcc) γ-austenite transforms into hexagonal close-packed (hcp) ε-martensite and/or body-centered cubic (bcc) α'-martensite. The amount of ε- and α'-martensites formed during deformation process strongly depends on the chemical composition of the alloy, the type and level of plastic straining as well as the temperature of deformation [9-11]. Martensitic transformations in 301LN and 316L steels were compared by Abreu et al. [10]. Both alloys were deformed by CR to 5, 26 and 47% reduction in thickness. The 301LN steel exhibited

direct martensitic transformation from γ-austenite to α'-martensite. The volume fraction of α'-martensite phase increased with increasing strain, reaching 60% for the thickness reduction of 47%. At the same time, 316L steel contained only 8% α'-martensite at the same level of CR. Another study has also proved a better stability of austenite phase in 316L steel, since martensitic transformation was not observed even after CR to a thickness reduction of 60% [11].

Beside the chemical composition, another important factor influencing the martensitic transformation is the deformation temperature. Former studies revealed that the occurrence of martensitic transformation in 316L steel is more probable at lower temperatures of plastic deformation, and at room temperature large strains are required for the observation of a phase transformation [8,9,12,13]. The martensitic transformation in 316L steel processed by HPT within a temperature range between -196 °C and 720 °C have been recently investigated by Scheriau et al. [9]. At deformation temperatures lower than 20 °C ε-martensite was formed from the austenite phase, while α'-martensite was not observed at any deformation temperature. The martensitic transformation sequence γ→ε→α' was also observed in severely deformed austenitic steels [11,14,15].

The present work investigates the influence of plastic deformation route on phase composition, microstructure and hardness of 316L stainless steel. Two different deformation methods, CR and HPT, were used for plastic straining of a coarse-grained initial austenite structure. The grain size, dislocation density and twin-fault probability were determined in the main phase of the plastically deformed microstructures.

Material processing and experimental techniques

The chemical composition of the 316L austenitic stainless steel used in this study is presented in Table 1. In order to obtain a single phase γ-austenite with homogeneous microstructure, the material was heat-treated at 1100 °C for 1 hour, followed by quenching in water to room temperature. A sheet was cold rolled to 20% reduction in thickness. The specimen prepared from this sheet is denoted as sample CR. For HPT-processing, disks were cut from the quenched material with a diameter of ~9.85 mm and a thickness of ~0.85 mm. The disks were processed by HPT at room temperature under quasi-constrained conditions at a rate of 1 rpm and a pressure of 6.0 GPa for N=½ and 10 turns [16].

An FEI Quanta 3D scanning electron microscope (SEM) was utilised to study the microstructure on the cross-sections of samples deformed by CR and HPT. The sample surface was first mechanically polished and finally electro-polished at 28 V and 0.5 A using an electrolyte with a composition of 70% ethanol, 20% glycerine and 10% perchloric acid (in vol. %). Electron backscatter diffraction (EBSD) images were taken on the initial and the deformed samples with a step size of 30 nm. The microstructure was also studied by transmission electron microscopy (TEM) performed by a Philips CM20 electron microscope operating at 200 keV. Thin foil specimens were prepared from the cross-sections of the CR sheet and the HPT disks. The images and the diffraction patterns were recorded on imaging plates and the diffraction patterns were indexed using the Process Diffraction Program [17].

The phase composition, the crystallite size, the dislocation density and the twin-fault probability were analyzed by X-ray diffraction (XRD). The XRD patterns were measured using a high-resolution diffractometer with monochromated $CoK_{\alpha 1}$ (λ= 0.1789 nm) radiation. The X-ray line profile analysis (XLPA) was carried out by the Convolutional Multiple Whole Profile (CMWP) fitting procedure described elsewhere [18]. In this method, the measured diffraction pattern is fitted by the sum of a background spline and the convolution of the instrumental pattern and the theoretical functions related to the crystallite size, dislocations and twin-fault. As a result of the fitting, the area-weighted mean crystallite size ($\langle x \rangle_{area}$), the dislocation density (ρ) and the twin-fault probability (β) were obtained.

The Vickers hardness (HV) was measured by a Zwick Roell ZHμ microhardness tester with an applied load of 500 g and a dwell time of 10 s.

Table 1: The concentrations of the main alloying elements as determined by energy-dispersive X-ray spectroscopy for 316L steel used in this study.

Element	Fe	Cr	Ni	Mo	Mn	Si	Cu	Co
wt.%	Bal.	17.20	8.97	2.13	1.03	0.77	0.48	≤ 0.35

Results and discussion

Phase composition. Fig. 1 shows the X-ray diffractograms obtained for the initial material, sample CR, as well as for the centre and the periphery of the HPT-processed disks. It is revealed that almost the whole initial material is γ-austenite containing a very small fraction of secondary phase α'-martensite (~3 vol.%). No martensitic transformation was observed after CR for 20% reduction in thickness (see Fig. 1b). On the other hand, HPT resulted in a phase transformation from γ-austenite into ε and α'-martensites. EBSD investigations (not shown here) revealed that in the centre of the sample processed by ½ turn of HPT, bands of ε-martensite phase formed inside the γ-austenite grains [19]. Then, α'-martensite crystallites were nucleated in the ε-martensite bands. Therefore, the phase transformation in the HPT-processed samples appears to follow the sequence γ→ε→α'.

Fig. 1 shows that the higher the strain, the more advanced the martensitic transformation. With increasing both the distance from the center and the number of turns, the sum of the volume fractions of ε- and α'-martensites increases. Although in the centre of the HPT disks the torsional strain is theoretically zero [20], a phase transformation was observed which is due to the compressive strain caused by the large external load (~6 GPa). After 10 turns of HPT the disk periphery contains mainly α'-martensite (see Fig. 1b).

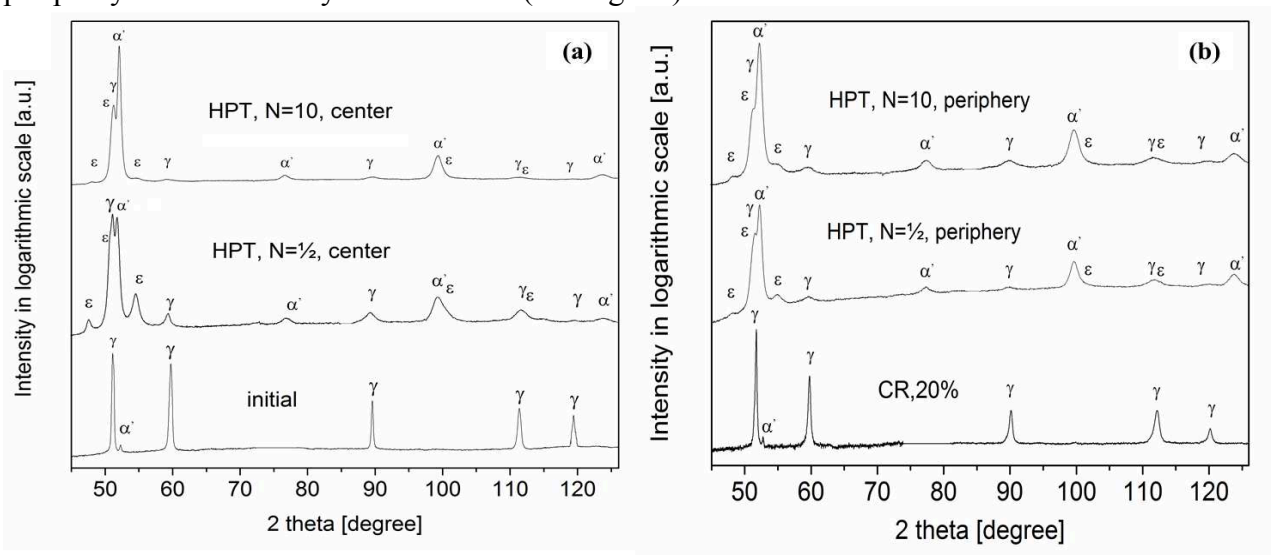

Fig. 1: X-ray diffractograms obtained for (a) the initial sample and the centre of the disks processed by HPT for ½ and 10 turns, and (b) sample CR and the periphery of the disks processed by HPT for ½ and 10 turns.

Microstructure of the plastically deformed samples. EBSD images (not shown here) revealed that the mean grain size decreased from ~42 μm to ~26 μm during CR without the formation of new phases. The TEM image in Fig. 2a shows that inside the γ-austenite grains twin boundaries were formed due to the low stacking-fault energy (SFE) of 316L steel. The average twin-spacing is ~50 nm. EBSD studies indicate that in the centre of the disk processed for ½ turn of HPT a lamellar microstructure containing γ-, ε- and α'- phases was formed. The formation of ε-martensite is also related to the low SFE of 316L steel as this phase can be formed by developing stacking faults on every second {111} plane in fcc γ-austenite [21]. Therefore, it can be concluded that the effect of the low SFE on the development of microstructure is different in the two ways of deformation.

During CR only twin boundaries were formed while HPT yielded a phase transformation. Most probably, the high pressure applied in HPT-processing facilitated the formation of ε-martensite, since this phase is a high-pressure modification of iron [22].

The bright-field TEM image in Fig. 2b shows that at the centre of the disk processed by HPT for ½ turn the microstructure is distorted due to the high density of dislocations and stacking faults. With increasing the number of turns to 10 the grain size in the disk center was refined to 95 nm, as revealed by dark-field TEM images (not shown here) [19]. It was observed that the grain refinement was faster at the periphery than in the center of the disks. According to the dark-field TEM images, the grain size values at the periphery after ½ and 10 turns were 105 and 45 nm, respectively.

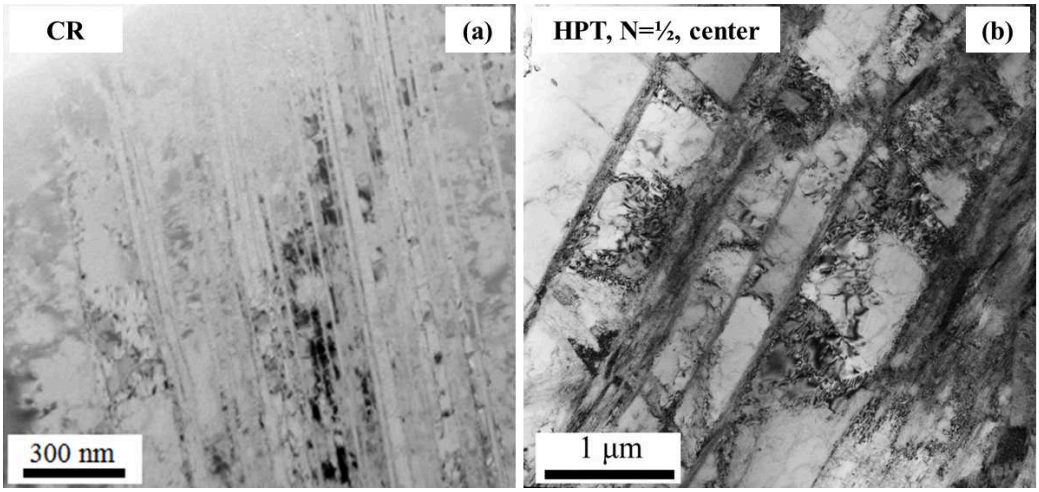

Fig. 2: Bright field TEM images for (a) sample CR and (b) the centre of the disk processed by HPT for ½ turn.

The parameters of microstructure obtained by XLPA are listed in Table 2. The dislocation density is high (~10 × 10^{14} m^{-2}) even if the thickness reduction is only 20% in the CR process. The twin-fault probability is ~0.5 % which corresponds to an average twin-boundary spacing of ~42 nm. This value is in reasonable agreement with the twin boundary spacing estimated from the TEM images (~50 nm). The crystallite size determined by XLPA (~90 nm) is much smaller than the grain size obtained by EBSD (~26 μm) for sample CR. This difference can be explained by the fact that XLPA measures the size of the sub-grains or dislocation cells rather than the true grain size.

For the HPT-processed disks, the diffraction peaks of the different phases strongly overlap which makes XLPA difficult. However, at the periphery of the disks the majority of material is α'-martensite, therefore the peaks of other phases can be put into the pattern background. Therefore, the parameters of the microstructure were determined by XLPA only for the bcc α'-martensite phase at the disk periphery (see Table 2). It was found that the crystallite size and the dislocation density were much smaller and higher, respectively, at the periphery of the HPT-processed disks than in sample CR due to the much larger plastic strain. The crystallite size remained unchanged within the experimental error while the dislocation density increased from ~73 × 10^{14} m^{-2} to ~133 × 10^{14} m^{-2} with increasing numbers of HPT turns from ½ to 10.

Hardness measurement. The hardness values for the initial material and the samples processed by CR and HPT are listed in Table 2. The hardness of the initial material was ~1410 MPa. After CR the hardness increased to ~2600 MPa. The hardness increment in the HPT-processed samples was larger due to the smaller grain size and the higher dislocation density. It is noted that the hardness increased with increasing both the numbers of revolutions and the distance from the disk centre. After ½ turn of HPT the hardness increased with factors of ~2.8 and ~3.7 in the centre and periphery, respectively. When the numbers of revolutions increased to 10 the hardness reached ~5150 and ~6130 MPa at the centre and periphery of the disk, respectively. The smaller the grain size and the higher the dislocation density, the larger the hardness for the HPT-processed samples.

Table 2: The grain size obtained by EBSD or TEM, the hardness and the parameters of the microstructure determined by X-ray line profile analysis for the main phase in the initial and deformed samples. $\langle x \rangle_{area}$ is the area-weighted mean crystallite size, ρ is the dislocation density and β is the twin-fault probability.

sample	Main phase	Grain size	$\langle x \rangle_{area}$ (nm)	ρ (10^{14} m^{-2})	β (%)	Hardness (MPa)
Initial	γ-austenite	42 ± 4 μm EBSD	-----	-----	-----	1410 ± 50
CR, 20%	γ-austenite	26 ± 3 μm EBSD	90 ± 10	10 ± 1	0.5 ± 0.1	2600 ± 70
HPT, N=½, periphery	α'-martensite	105 ± 8 nm TEM	27 ± 1	73 ± 8	-----	5150 ± 160
HPT, N=10, periphery	α'-martensite	45 ± 4 nm TEM	22 ± 2	133 ± 12	-----	6130 ± 190

4. Conclusions

Coarse-grained 316L stainless steel with a γ-austenite structure was plastically deformed by CR and HPT. The phase composition and the microstructure of the deformed samples were compared and the following conclusions were drawn from the results:

1. No martensitic transformation was observed in the sample processed by CR for 20% reduction in thickness. In this specimen the grain size was refined from ~42 μm to ~26 μm and large numbers of twin boundaries were formed inside the grains. At the same time, in the HPT-processed samples γ-austenite was gradually transformed into ε- and α'-martensites. ε- martensite was only an intermediate phase and at the periphery of the disk processed by 10 turns of HPT the majority of the material was α'-martensite. The grain size in this sample was refined to a very small value of ~45 nm.
2. An XLPA investigation of γ-austenite in specimen CR revealed that the crystallite size was ~90 nm and the dislocation density was $\sim 10 \times 10^{14}$ m^{-2} already after 20% reduction in thickness. The high density of twin-faults detected by TEM was in accordance with XLPA results. The HPT-processed samples exhibited much smaller crystallite size and higher dislocation density than specimen CR. At the periphery of the disk processed by 10 turns the crystallite size and the dislocation density in α'-martensite phase were ~22 nm and $\sim 133 \times 10^{14}$ m^{-2}, respectively.
3. The deformation by CR resulted in a two-fold increment in hardness to ~2600 MPa. HPT-processing yielded much larger hardness at the disk periphery for both ½ and 10 turns due to the much smaller grain size and higher dislocation density. A very high hardness of ~6130 MPa was achieved at the periphery of the disk processed by 10 turns of HPT.

Acknowledgements

This study was supported by the Hungarian Scientific Research Fund, OTKA, Grant No. K-109021. The authors are grateful to Mr. Gabor Varga for the SEM and EBSD investigations. The first author was supported by the executive program between the Egyptian and the Hungarian Governments. YH and TGL were supported by the European Research Council under ERC Grant Agreement No. 267464-SPDMETALS.

References

[1] W.G. Kim, S.N. Yin, W.S. Ryu, C.B. Lee, Application of Minimum Commitment Method for Predicting Long-Term Creep Life of Type 316LN Stainless Steel, Korean Inst. Met. Mater. 46 (2008) 118-124.
[2] Y. Kim, Y. Kim, D. Kim, S. Kim, W. Nam, H. Choe, Effects of Hydrogen Diffusion on the Mechanical Properties of Austenite 316L Steel at Ambient Temperature, Mater. Trans. 52 (2011) 507-513.
[3] I. Gotman, Characteristics of Metals Used in Implants, Endourology 11 (1997) 383-389.
[4] G.L. Lucas, F.W. Cooke, E.A. Friis, A Primer of Biomechanics, A primer of biomechanics, Springer Science + Business Media, New York, NY, 1999.
[5] R.Z. Valiev, Y. Estrin, Z. Horita, T.G. Langdon, M.J. Zehetbauer, Y.T. Zhu, Producing Bulk Ultrafi ne-Grained Materials by Severe Plastic Deformation, JOM 58(4) (2006) 33-39.
[6] T.G. Langdon, Twenty-five years of ultrafine-grained materials: Achieving exceptional properties through grain refinement Acta Mater. 61 (2013) 7035-7059.
[7] S.S.M. Tavaresa, D. Fruchart, S. Miraglia, A magnetic study of the reversion of martensite α' in a 304 stainless steel, J. Alloys Compd. 307 (2000) 311-317.
[8] K. Spencer, M. Véron, K. Yu-Zhang, J.D. Embury, The strain induced martensite transformation in austenitic stainless steels, Part 1- Influence of temperature and strain history, Mater. Sci. Techn. 25 (2009) 7-17.
[9] S. Scheriau, Z. Zhang, S. Kleber, R. Pippan, Deformation mechanisms of a modified 316L austenitic steel subjected to high pressure torsion, Mater. Sci. Eng. A 528 (2011) 2776-2786.
[10] H.F.G. Abreu, S.S. Carvalho, P.L. Neto, R.P. Santos, V.N. Freire, P.M.O. Silva, S.S.M. Tavares, Deformation Induced Martensite in an AISI 301LN Stainless Steel: Characterization and Influence on Pitting Corrosion Resistance, Mater. Res. 10 (2007) 359-366.
[11] Y. Mine, Z. Horita, Y. Murakami, Effect of hydrogen on martensite formation in austenitic stainless steels in high-pressure torsion, Acta Mater. 57 (2009) 2993-3002.
[12] K. Spencer, J.D. Embury, K.T. Conlon, M. Véron, Y. Bréchet, Strengthening via the formation of strain-induced martensite in stainless steels, Mater. Sci. Eng. A 387-389 (2004) 873-881.
[13] C. Garion, B. Skoczeń, S. Sgobba, Constitutive modelling and identification of parameters of the plastic strain-induced martensitic transformation in 316L stainless steel at cryogenic temperatures, Int. J. Plast. 22 (2006) 1234-1264.
[14] J.A. Venables, The martensite transformation in stainless steel, Phil. Mag. 7 (1962) 35-44.
[15] P.L. Mangonon, G. Thomas, The Martensite Phases in 304 Stainless Steel, Metall. Trans 1 (1970) 1577-1586.
[16] R.B. Figueiredo, P.R. Cetlin, T.G. Langdon, Using finite element modeling to examine the flow processes in quasi-constrained high-pressure torsion, Mater. Sci. Eng. A 528 (2011) 8198-8204.
[17] J.L. Lábár, Electron Diffraction Based Analysis of Phase Fractions and Texture in Nanocrystalline Thin Films, Part III: Application Examples, Microsc. Microanal. 18 (2012) 406-420.
[18] G. Ribárik, J. Gubicza, T. Ungár, Correlation between strength and microstructure of ball-milled Al–Mg alloys determined by X-ray diffraction, Mater. Sci. Eng. A 387-389 (2004) 343-347.
[19] J. Gubicza, M. El-Tahawy, Y. Huang, H. Choi, H. Choe, J.L. Lábár, T.G. Langdon, Microstructure, phase composition and hardness evolution in 316L stainless steel processed by high-pressure torsion, Mater. Sci. Eng. A 657 (2016) 215-223.
[20] A.P. Zhilyaev, T.G. Langdon, Using high-pressure torsion for metal processing: Fundamentals and applications, Prog. Mater. Sci. 53 (2008) 893-979.
[21] S. Martin, C. Ullrich, D. Šimek, U. Martin, D. Rafaja, Stacking fault model of ε-martensite and its DIFFaX implementation, J. Appl. Cryst. 44 (2011) 779-787.
[22] R.L. Clendenen, H.G. Drickamer, The effect of pressure on the volume and lattice parameters of Ruthnium and Iron, Phys. Chem. Solids 25 (1964) 865-868.